Article

Journal of
Nanoscience and Nanotechnology
Vol. 19, 721–728, 2019
www.aspbs.com/jnn

mpg-C_3N_4/Ag_2O Nanocomposites Photocatalysts with Enhanced Visible-Light Photocatalytic Performance

Zhe Jiang, Shukun Le, Yingjie Xie, Qiuyan Huang, Bin Wang, and Tingshun Jiang*

School of Chemistry and Chemical Engineering, Jiangsu University, Zhenjiang 212013, Jiangsu, China

To study the photocatalytic activity under visible light irradiation, a series of mesoporous graphitic carbon nitride (mpg-C_3N_4)/Ag_2O photocatalysts were synthesized. The as-prepared photocatalysts were characterized with X-ray diffraction (XRD), scanning electron microscopy (SEM), transmission electron microscopy (TEM), N_2 adsorption Brunauer-Emmett-Teller method (N_2-BET), Fourier transform infrared spectroscopy (FT-IR), UV-vis diffuse reflectance spectra (DRS), and photoluminescence spectra (PL) methods to determine their phase structure, purity, morphology, spectroscopic and photoluminescence emission performance, respectively. Photocatalytic degradation of methyl orange (MO) aqueous solution under visible-light irradiation indicated that the mpg-C_3N_4/Ag_2O-50 nanocomposite exhibited the best activity. The degradation rate of MO reached to 90.8% in 120 min onto the mpg-C_3N_4/Ag_2O-50 nanocomposite, and as compared with the pure mpg-C_3N_4 and Ag_2O samples, the photocatalytic activity of the mpg-C_3N_4/Ag_2O-50 nanocomposite was greatly enhanced. The enhancement of photocatalytic activity was mainly ascribed to the enhanced visible-light absorption ability and the formation of *p–n* heterojunctions between counterparts of the nanocomposites, which promoted the generation and separation of charge carriers.

Keywords: mpg-C_3N_4/Ag_2O, *p–n* Heterojunctions, Visible-Light Photocatalysis, Photocatalytic Activity, MO Degradation.

1. INTRODUCTION

Due to the great industrial and population growth, the environmental pollution is becoming one of the biggest challenges facing human being worldwide.[1–5] TiO_2, as the first and most investigated semiconductor, works only with ultraviolet (UV) radiation which does not satisfy the requirement of visible-light-driven applications.[6–8] In spite of the success of metal oxide catalysts for photochemistry applications, there remains the universal problem that most metal oxides only utilize particular UV light that accounts for ∼4% of total solar irradiation on the earth. Developing the photocatalysts with visible light response has attracted much attention.[9–11] These days, heterogeneous photocatalytic processes is used in widespread applications of pollutants degradation both in liquid and gaseous regime. There is potentially advantageous, such as it proceeds at ambient conditions resulting in complete mineralization of organic pollutants to harmless products like CO_2, H_2O and mineral acids.[12, 13]

Recently, a polymeric carbon nitride (C_3N_4) material was introduced as a metal-free photocatalyst for visible-light-driven application. The C_3N_4 material is composed of carbon, nitrogen, and some minor hydrogen content only.[14] New opportunities has been offered by the organic semiconductor C_3N_4 materials based photocatalysis due to its multifunctional properties like photochemical stability, highest light conversion efficiency, favorable band edge positions, cheap availability, low cost, non-toxicity, high stability, and especially its intrinsic visible light response.[15–18] On the other hand, the C_3N_4 is a cheap and clean photocatalyst, and shows suitable band gap to spectral response. However, the low electrical conductivity of C_3N_4 limited its photocatalytic application. Increasing its conductivity is vital to reduce the recombination. Mesoporous materials such as mesoporous carbon-based materials with high electron conductive ability were introduced into C_3N_4 system, which can enhance the separation of photogenerated carriers, and thus improve the photocatalytic activity.[19] Also, heterogeneous photocatalysis with g-C_3N_4 is potentially advantageous because of its intrinsic organic nature, thus allowing its electronic band gap

*Author to whom correspondence should be addressed.

structure to be tuned, and it proceeds at ambient conditions resulting in complete mineralization of organic pollutants to harmless products like CO_2, H_2O and mineral acids.[20] Recent studies have shown that the light response and photocatalytic activity of the mesoporous g-C_3N_4 (mpg-C_3N_4) materials can be improved. It has been successfully prepared by templating methods, such as soft-templating and hard-templating methods.[21–24] Compared with the pure g-C_3N_4, the mpg-C_3N_4 modify the electronic properties and extend its optical absorption to the visible region, and enhanced its photocatalytic activity, also possessed a larger number of active sites on the surface, which can show potential in an even wider range of application.

On the other hand, Ag_2O has been reported as the best candidate because of its high solubility, larger ionic size, and minimum orbital energy. Ag_2O as a classical *p*-type semiconductor has been focused much interest. The Ag_2O has the narrow energy bandgap,[25] which has the ability to absorb a large part of visible light. Ag_2O nanoparticles as a promising photocatalyst with high photocatalytic performance, it has been widely used to tune the light response of some wide bandgap semiconductors into the visible region and enhance their photocatalytic activities. Many studies on the synthesis of Ag_2O composite photocatalysts have been reported, such as Ag_2O/TiO_2,[26] Ag_2O/ZnO,[27] Ag_2O/Bi_2O_3,[28] Ag_2O/Ag_2CO_3,[29] and so forth. Thus, it is possible to improve the photocatalytic activity of *n*-type mpg-C_3N_4 by fabricating mpg-C_3N_4/Ag_2O *p–n* heterojunction photocatalysts due to its well matched overlapping band structure. The *p–n* heterojunction will bring more effective interface transfer of photo-generated electrons and holes in comparison with the traditional composites.

Herein, mpg-C_3N_4/Ag_2O nanocomposites and their excellent photocatalytic activities for degrading methyl orange (MO) under visible light irradiation are reported to draw new prospects in this domain. The facile preparation of mpg-C_3N_4/Ag_2O *p–n* heterojunction was synthesized by a simple liquid phase reaction at room temperature. The crystal structure and morphology of the prepared samples were discussed in detail. The photocatalytic activities were tested by varying the mpg-C_3N_4/Ag_2O nanocomposites weight ratios to find the highest photocatalytic activities. The novel hetero-structured photocatalysts possessed better photocatalytic activity and stability toward the degradation of methyl orange (MO) under visible light irradiation as compared to the pure mpg-C_3N_4 and Ag_2O. Meanwhile, account of the experimental results, the detailed possible mechanism for the enhanced activity of mpg-C_3N_4/Ag_2O nanocomposites was also discussed.

2. EXPERIMENTAL DETAILS

2.1. Materials

The chemicals used in this work, melamine, silver nitrate ($AgNO_3$), sodium hydroxide (NaOH), hydrochloric acid, sulfuric acid, hydrofluoric acid, tetraethyl orthosilicate, were purchased from Medicines Group. Copolymers P123 was purchased from Aldrich Company, and methyl orange (MO) was commercially available from Beijing Dye Processing. All chemical reagents in this study were of analytical grade. SBA-15 was prepared using P123 as a template and tetraethyl orthosilicate as silicon source according to our previous publication.[30]

2.2. Synthesis of mpg-C_3N_4

Typically, 2 g of melamine, 0.28 g concentrated sulfuric acid and 1 g of SBA-15 were added into deionized water to obtain a suspension. Then, the suspension was sonicated for 30 min, and stirred for 6 h at 70 °C. After that, the mixture was transferred into a stainless steel autoclave with a Teflon liner of 100 mL capacity, and placed in an oven at 100 °C for 6 h, heated at 160 °C for 6 h. After cooling to the ambient temperature, the prepared product was washed with deionized water by suction filtration until the filtrate is neutral. Subsequently, dried at 60 °C for 24 h and the dried sample was transferred into a tube furnace, and heated to 550 °C at a heating rate 2 °C/min under N_2 flow and kept at 550 °C for 4 h. After cooling to room temperature, the calcined sample was impregnated with 5 wt% hydrofluoric acid at room temperature for 24 h to remove the SBA-15 template. After that, the sample was washed repeatedly with deionized water, and dried at 60 °C for 12 h in an oven. Finally, a powder was obtained. The calcined sample was denoted as mpg-C_3N_4.

2.3. Fabrication of mpg-C_3N_4/Ag_2O Nanocomposite Photocatalysts

mpg-C_3N_4 was added into 35 mL of deionized water and sonicated for 30 min. Then, 0.4 g to $AgNO_3$ was added into the suspension and stirred for 30 min. After that, 15 mL of 0.4 g NaOH was added drop by drop under stirring. All the experiments were carried out at room temperature. After stirring for 4 h, the obtained precipitate was collected by centrifugation and washed with deionized water for three times. Finally, the solid product was dried at 60 °C for 12 h in an oven. A series of mpg-C_3N_4/Ag_2O nanocomposites with different mass ratios of mpg-C_3N_4 and Ag_2O were prepared by changing the amounts of mpg-C_3N_4 and marked as mpg-C_3N_4/Ag_2O-*x*, where *x* represented the mpg-C_3N_4 weight percent in the composites. As a reference, the pure Ag_2O was prepared without adding mpg-C_3N_4 under the same conditions.

2.4. Catalyst Characterization

Powder X-ray diffraction (XRD) was carried out with a Japan Shimadzu XRD-6100Lab X-ray diffractometer (Cu Kα, 40 kV, 40 mA), with radiation between 5∼80°, and with a scan rate of 4°/min. Fourier Transform Infrared (FT-IR) spectra were recorded on American Nicolet FT-IR spectrometer (Nexus FT-IR 470) with KBr pellet technique

and the range is 4000–400 cm^{-1}. The morphologies and microstructures of the samples were observed on a JEOL JSM-6700F scanning electron microscopy (SEM). Transmission electron microscopy (TEM) images were obtained on a JEM-2010F electron microscope (JEOL, Japan) with an acceleration voltage of 200 kV. The specific surface areas and pore sizes were measured by a Quantachrome NOVA2000e instrument (USA). The specific surface areas of the samples were obtained using the Brunauer-Emmett-Teller (BET). The optical diffuse reflectance spectra (UV-vis) were measured on a PerkinElmer Lambda 750 s UV-vis-NIR spectrometer equipped with an integrating sphere. $BaSO_4$ was used as the reference material, and the polycrystalline samples were ground well before the measurement. The photoluminescence (PL) spectra of the samples were recorded on a Varian Cary Eclipse spectrometer at an excitation wavelength of 375 nm.

2.5. Photocatalytic Performance Test

Photocatalytic activity of the mpg-C_3N_4/Ag_2O samples was evaluated by photocatalytic degradation of MO aqueous solution under visible-light irradiation. In each experiment, 50 mg of photocatalysts was added into 100 mL of MO solution (10 mg/L). Before light irradiation, the suspensions were magnetically stirred in the dark for 30 min to ensure the adsorption–desorption equilibrium between MO molecules and the photocatalysts reaches. Then, a 350 W tungsten lamp with a cutoff filter ($\lambda > 400$ nm) was used as the visible-light source. At 20 min intervals, a 4 mL solution was sampled and centrifuged to remove the photocatalyst particles, and its absorbance was detected using a UV-vis spectrometer at 464 nm. To estimate the photostability of the photocatalysts, the sample after one trial was collected through centrifugation, washed with deionized water and dried for the subsequent cycle test.

3. RESULTS AND DISCUSSION

3.1. Characterization

XRD patterns of mpg-C_3N_4, Ag_2O, and the as-prepared mpg-C_3N_4/Ag_2O composites with different mass ratios are shown in Figure 1. It is well known that mpg-C_3N_4 is based on tri-s-triazine building blocks.[31] The strong peak at $2\theta = 27.4°$ corresponding to the characteristic interplanar stacking peak (002) of an aromatic system was observed.[32] The small angle peak at 13.0° is associated with interlayer stacking.[33] The observed diffraction peaks of pure Ag_2O are in good agreement with those reported in the literatures for pure cubic Ag_2O.[25, 34] The diffraction peak (002) is a characteristic peak of g-C_3N_4 that was also present in pattern of the mpg-C_3N_4/Ag_2O nanocomposite. It was also seen that the crystal phase of Ag_2O did not change after hybridization with mpg-C_3N_4, but the diffraction peak positions for Ag_2O were located at slightly lower

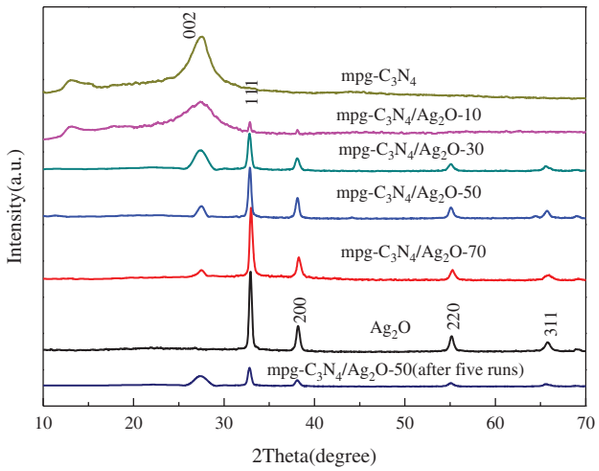

Figure 1. XRD patterns of mpg-C_3N_4, Ag_2O, the synthesized mpg-C_3N_4/Ag_2O nanocomposites and mpg-C_3N_4/Ag_2O-50 (after five runs) sample.

angles than those for pure Ag_2O, suggesting a strong interaction between mpg-C_3N_4 and Ag_2O. No other impurity phase was seen, indicating the mpg-C_3N_4/Ag_2O to be a two-phase composite. Moreover, we found from Figure 1 that the diffraction peaks of the mpg-C_3N_4/Ag_2O-50 sample after five runs weakened as compared with the parent mpg-C_3N_4/Ag_2O-50 sample.

Figure 2 shows the FT-IR spectra of the pure mpg-C_3N_4, pure Ag_2O, and the mpg-C_3N_4/Ag_2O-50 composite photocatalysts, respectively. For the pure mpg-C_3N_4, the broad band around 3200 cm^{-1} is indicative of the N–H stretching vibration modes. Several bands in the 1220–1660 cm^{-1} region were found, which correspond to the typical stretching modes of CN heterocycles, and the sharp band at 810 cm^{-1} is related to the breathing mode of the triazine units.[32, 35–37] For the pure Ag_2O, the broad Ag–O band vibration at around 600 cm^{-1} is clearly visible.[34] The characteristic peaks of mpg-C_3N_4 and Ag_2O are retained in the mpg-C_3N_4/Ag_2O composite samples. The FT-IR spectra of the mpg-C_3N_4/Ag_2O composites represent the overlap of the spectra of both mpg-C_3N_4 and Ag_2O.

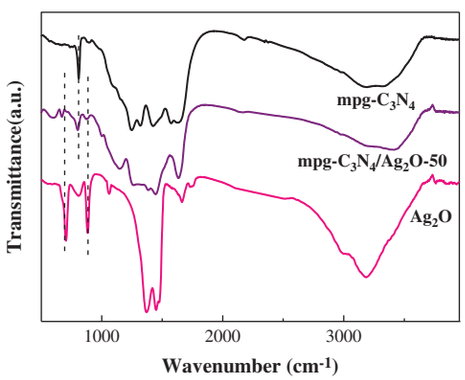

Figure 2. FT-IR spectra of mpg-C_3N_4, Ag_2O, and the synthesized mpg-C_3N_4/Ag_2O nanocomposites.

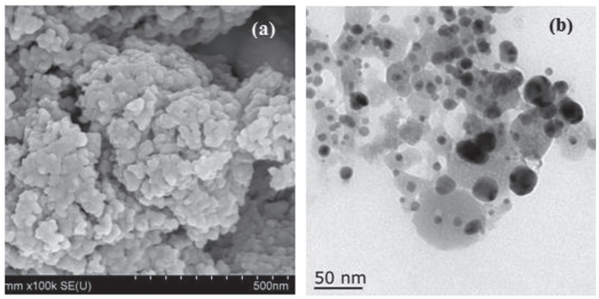

Figure 3. SEM images of the mpg-C_3N_4/Ag_2O-50 (a) and TEM images of the mpg-C_3N_4/Ag_2O-50 (b).

Figure 3 shows SEM and TEM images of the mpg-C_3N_4/Ag_2O-50 nanocomposite samples. The surface morphology of the synthesized mpg-C_3N_4/Ag_2O-50 seemed not to be smooth, consisting of particles on the sheets. Indeed, the sheet-like morphology was confirmed by TEM observations of the g-C_3N_4 (Fig. 3(b)). The morphology of the synthesized g-C_3N_4 was due to aggregation and gathering of the g-C_3N_4 sheets. After the introduction of Ag_2O, the dark part of the lamellar mpg-C_3N_4 is appeared of Ag_2O particles and the size of Ag_2O particles is about 5–35 nm. A lot of Ag_2O particles are attached to the surface of mpg-C_3N_4 strongly. According to the Ref. [38], the pure Ag_2O nanoparticles had a particle size of 100–200 nm, and a grain-like morphology with polygonal grain shapes. The addition of mpg-C_3N_4 can greatly improve the decentralized of Ag_2O particles and efficiently decrease the particle size of Ag_2O. The results of the SEM and TEM images also clearly reveals a close interface between the mpg-C_3N_4 and Ag_2O in the as-prepared composite and indicates the formation of heterojunction,[39] which is significant for separating the photo-generated electron–hole pairs and thus improving the quantum efficiency.

Figure 4 shows the UV-vis diffuse reflectance spectroscopy spectra of pure mpg-C_3N_4, pure Ag_2O, and the mpg-C_3N_4/Ag_2O nanocomposite samples. Conventional carbon nitride shows the typical absorption pattern of

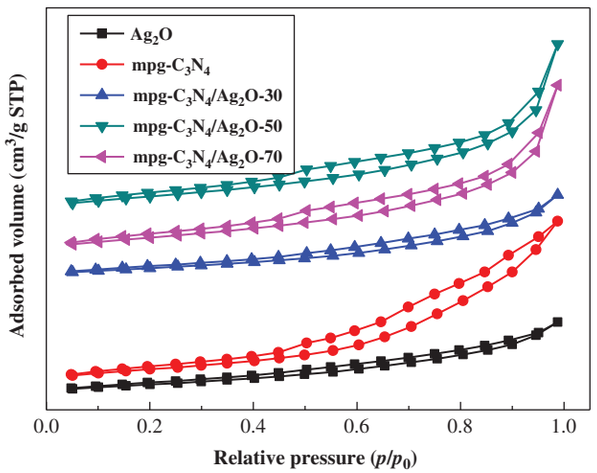

Figure 5. Nitrogen adsorption–desorption isotherms of mpg-C_3N_4, Ag_2O and mpg-C_3N_4/Ag_2O nanocomposites.

an organic semiconductor with very strong adsorption at about 460 nm.[14] After the introduction of Ag_2O nanoparticles on the surface of mpg-C_3N_4, the optical absorption of the composites in the visible region increases, while the absorption intensity of these composites is step-wisely strengthened with the increasing Ag_2O mass ratios. The absorption of the mpg-C_3N_4/Ag_2O nanocomposites within the visible-light range significantly increased, and a red shift in comparison with the pure mpg-C_3N_4 appeared. These results are attributed to the interaction between the mpg-C_3N_4 sheet and the Ag_2O nanoparticles in the composite system.[25,40] The enhanced light absorption of the mpg-C_3N_4/Ag_2O nanocomposite led to the generation of more photo-induced electron–hole pairs under visible-light irradiation, which subsequently resulted in enhanced photocatalytic activity. The Tauc plots of the $(Ah\nu)^{(1/2)}$ versus photon energy ($h\nu$) for the mpg-C_3N_4 and mpg-C_3N_4/Ag_2O-50 samples are displayed in Figure 4(b). The two intersections of the tangent lines and the horizontal axis denote the band gap energies of the synthesized

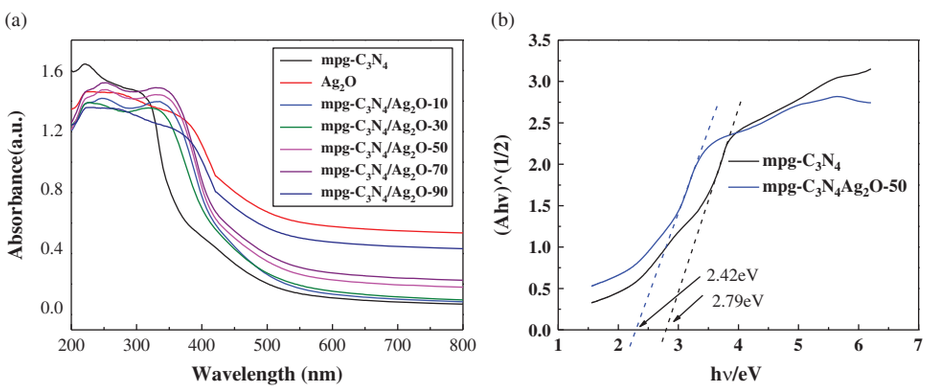

Figure 4. (a) UV-vis absorbance spectra of mpg-C_3N_4, Ag_2O, and the synthesized mpg-C_3N_4/Ag_2O nanocomposites and (b) $(Ah\nu)^{(1/2)}$ versus $h\nu$ curves of mpg-C_3N_4 and mpg-C_3N_4/Ag_2O-50 samples.

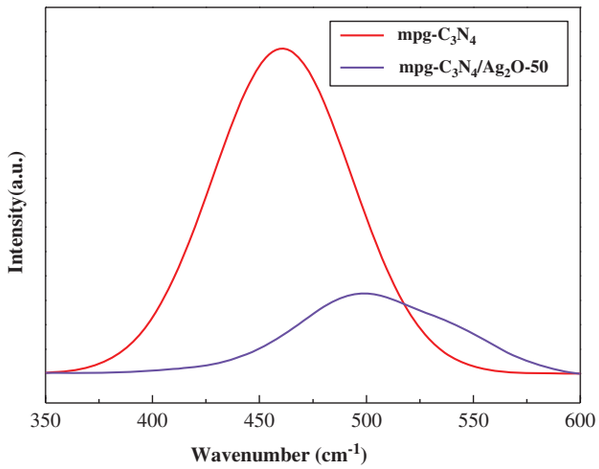

Figure 6. Photoluminescence emission spectra of mpg-C_3N_4 and the synthesized mpg-C_3N_4/Ag_2O-50 nanocomposites.

materials. As shown in Figure 4(b), the band gap energy (E_g) of the mpg-C_3N_4 and mpg-C_3N_4/Ag_2O-50 samples is 2.42 and 2.79 eV, respectively. As compared with the mpg-C_3N_4, the E_g of mpg-C_3N_4/Ag_2O-50 is small, suggesting that an easier trend for the mpg-C_3N_4/Ag_2O-50 to generate the electron–hole pairs by absorbing wider wavelength of light.

N_2 adsorption–desorption measurement is performed to investigate the textural properties of pure mpg-C_3N_4, Ag_2O, and as-prepared mpg-C_3N_4/Ag_2O nanocomposites and N_2 adsorption–desorption isotherms are shown in Figure 5. As can be seen in Figure 5, all mpg-C_3N_4/Ag_2O nanocomposites exhibited IV isotherms with H3 hysteresis loops[41, 42] at high relative pressure between 0.5 and 1.0, suggesting that the obtained samples have the mesoporous structure. Moreover, the type of H3 hysteresis loops is often observed on the aggregates of plate-like particles leading to slit-shaped pores which conformed to the sheet-like morphology (Fig. 3(a)). The surface area of mpg-C_3N_4/Ag_2O-50 calculated by BET method was 74.3 $m^2 \cdot g^{-1}$, which is much higher than that of the pure mpg-C_3N_4 (36.3 $m^2 \cdot g^{-1}$). Importantly, along with the apparent increment in surface area, facilitated charge separation in the composite system.

In order to disclose the effect of Ag_2O modification, PL spectral analysis was carried out to reveal the migration, transfer, and recombination processes of photoinduced electron–hole pairs in the composite system. All samples exhibit an emission peak centered at about 450 nm, which is similar to the reported value in the literatures.[34, 43] Figure 6 shows the PL spectra of pure mpg-C_3N_4 and the mpg-C_3N_4/Ag_2O-50 nanocomposites with an excitation wavelength of 365 nm at room temperature. As shown in Figure 6, the main emission peak is centered at about 460 nm for the pure mpg-C_3N_4 sample. The PL intensity of the mpg-C_3N_4/Ag_2O-50 nanocomposites is significantly decreased, indicating that the composite has a much lower recombination rate of photo-induced electron–hole pair.[34]

3.2. Photocatalytic Studies

The photocatalytic activity of pure mpg-C_3N_4, Ag_2O, and the as-prepared mpg-C_3N_4/Ag_2O nanocomposites for the degradation of MO under visible-light irradiation was evaluated (Fig. 7(a)). The initial concentration of the MO suspension was measured and used as the initial concentration C_0. The Y axis is reported as C/C_0, where C is the actual concentration of MO at the indicated reaction time. To disclose the adsorption effect of the catalyst on MO, the suspension was stirred for 30 min in the dark to achieve adsorption/desorption equilibration before the photo-degradation test. As can be clearly seen in Figure 7(a), the decrease in the concentration of MO is faster and more prominent with mpg-C_3N_4/Ag_2O nanocomposites than with pure mpg-C_3N_4 or Ag_2O under the same experimental conditions. Without the presence of a catalyst, the degradation of MO was negligible under visible-light irradiation, indicating the high stability of MO under visible-light irradiation. The results indicated that the presence of the catalyst and light is essential for the

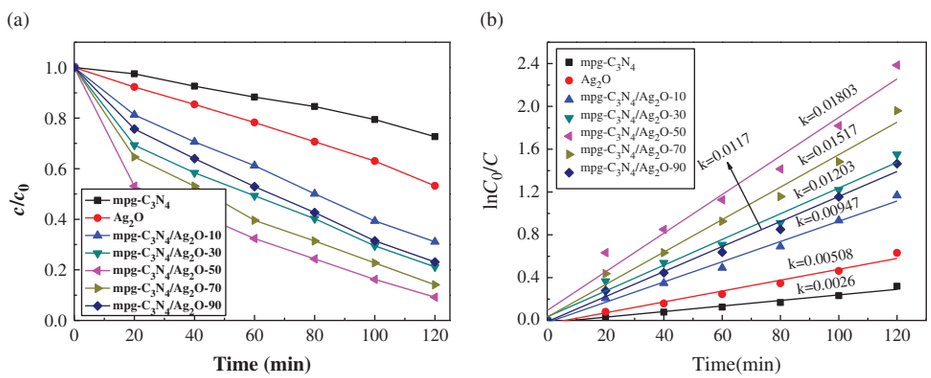

Figure 7. (a) Effect of various photocatalysts including pure mpg-C_3N_4, Ag_2O, and mpg-C_3N_4/Ag_2O nanocomposits on degradation efficiency of MO under visible light ; (b) The line plot of $\ln C_0/C$ versus time (light source: 350 W of tungsten lamp; catalyst dose: 0.05 g; reaction time: 120 min; $[MO]_{initial}$: 10 mg L^{-1}; volume 100 mL; 400 nm < λ < 680 nm).

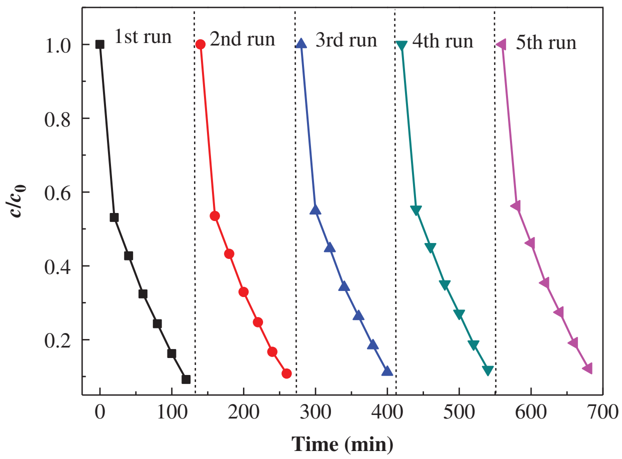

Figure 8. Recycling experiments of visible-light photocatalytic degradation of MO over the mpg-C_3N_4/Ag_2O-50.
Light source: 350 W of tungsten lamp; catalyst dose: 0.05 g; reaction time: 120 min; $[MO]_{initial}$: 10 mg L^{-1}; volume 100 mL; 400 nm < λ < 680 nm.

efficient degradation of MO under visible-light irradiation. Further, it is noted that after 120 min, the degradation rate of MO onto mpg-C_3N_4/Ag_2O-50 under visible-light irradiation is ca. 90.8%, which was much higher than that of pure mpg-C_3N_4. The enhanced photocatalytic performance of the mpg-C_3N_4/Ag_2O nanocomposite may be attributed to the synergistic effect between the interface of mpg-C_3N_4 and Ag_2O. Moreover, as displayed in the line plot of $\ln C_0/C$ versus time (Fig. 7(b)), it is noted that the photodegradation efficiency is in accordance with the Figure 7(a).

To study the stability of the as-prepared mpg-C_3N_4/Ag_2O photocatalyst, the used mpg-C_3N_4/Ag_2O-50 was collected, and the reusability was further examined in five successive MO degradation experiments. As shown in Figure 8, mpg-C_3N_4/Ag_2O-50 retained over 89% of its original photocatalytic activity after five successive experimental runs, which is also very important from a practical application point of view. The small loss might result from the loss of photocatalyst during recycling. Accordingly, the homogeneous hybridization between Ag_2O and mpg-C_3N_4 could prohibit the consumption of Ag_2O and enhance the activity and stability of the mpg-C_3N_4/Ag_2O nanocomposite photocatalysts, promising as visible-light-driven photocatalysts to practical applications of environmental protection.

In order to understand the mechanism on the enhanced photocatalytic activity of the mpg-C_3N_4/Ag_2O nanocomposite photocatalyst in depth, the active species generated during the process of mpg-C_3N_4/Ag_2O-photocatalyzed MO degradation are identified by free radical and hole trapping experiments. In this study, to investigate the role of these reactive species in the mpg-C_3N_4-Ag_2O system, tert-butyl alcohol (t-BuOH), EDTA and 1,4-benzoquinone (BQ) are used as the hydroxyl radical ($^{\cdot}OH$) scavenger, hole (h^+_{VB}) scavenger and superoxide radical ($^{\cdot}O_2^-$) scavenger, respectively.[44] Figure 9(a) displays the influence of various scavengers on the visible-light photocatalytic activity of mpg-C_3N_4/Ag_2O (represented by mpg-C_3N_4/Ag_2O-50) toward the degradation of MO and the line plot of $\ln C_0/C$ versus time was shown in Figure 9(b). It can be seen that when BQ was conducted as an $^{\cdot}O_2^-$ scavenger, a dramatic change in the photocatalytic activity was observed compared with the absence of scavenger, confirming that the dissolved O_2 has a clear effect on the photodegradation process under visible-light irradiation. Meanwhile, a similar change in the photocatalytic activity was observed upon the addition of t-BuOH as an $^{\cdot}OH$ scavenger. Nevertheless, the photodegradation of MO over the mpg-C_3N_4/Ag_2O can also be suppressed after the addition of EDTA as a hole (h^+_{VB}) scavenger compared with no scavenger under similar conditions. The above result indicates that h^+_{VB} is also the active species generated in the mpg-C_3N_4/Ag_2O photocatalytic system besides $^{\cdot}O_2^-$ and $^{\cdot}OH$ radical in the mpg-C_3N_4–Ag_2O system.

Based on the results above, a possible photocatalytic mechanism of the as-prepared mpg-C_3N_4/Ag_2O composites under visible light irradiation was proposed and

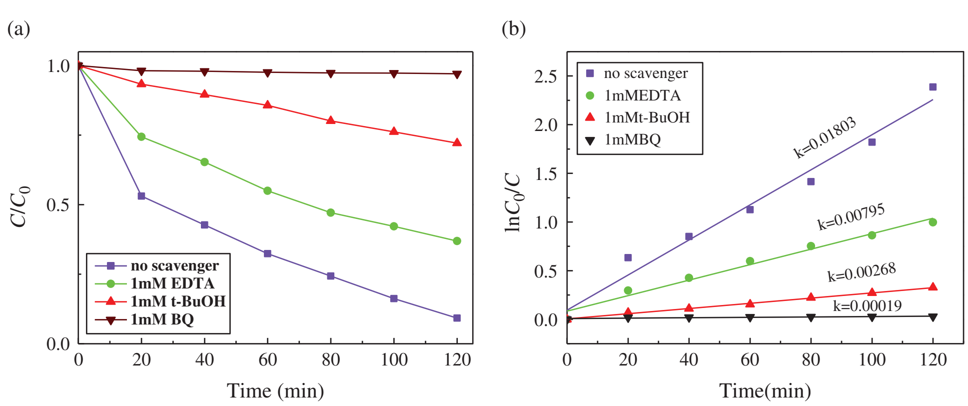

Figure 9. (a) Effect of various scavengers on the visible-light photocatalytic activity of mpg-C_3N_4/Ag_2O-50 toward the degradation of MO; (b) The line plot of $\ln C_0/C$ versus time.
Light source: 350 W of tungsten lamp; catalyst dose: 0.05 g; reaction time: 120 min; $[MO]_{initial}$: 10 mg L^{-1}; volume 100 mL; 400 nm < λ < 680 nm.

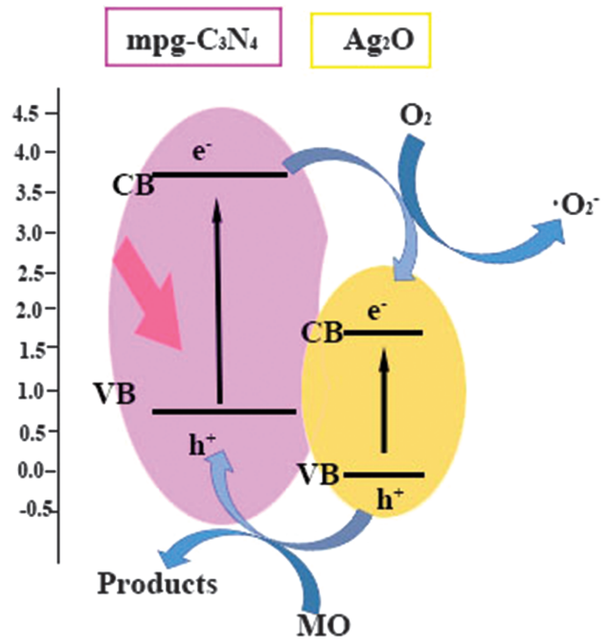

Scheme 1. A possible visible-light photocatalytic degradation diagram of mpg-C_3N_4/Ag_2O nanocomposite.

illustrated in Scheme 1. Under visible-light irradiation, the photo-induced electrons can easily be transferred from the conduction band (CB) of mpg-C_3N_4 to the CB of Ag_2O because the CB level of Ag_2O is lower than that of mpg-C_3N_4. Furthermore, because of the high conductivity of Ag_2O, the rate of electron transport is fast, which suppresses the direct recombination of photo-induced electron–hole pairs in the mpg-C_3N_4/Ag_2O hybrid composite system. Thus, Ag_2O acts as an acceptor of the photoinduced electrons from mpg-C_3N_4. Because of the presence of the mpg-C_3N_4/Ag_2O interface, the chance of recombination of photo-induced electron–hole pairs is further successfully suppressed, leaving more charge carriers to form reactive species. The electrons in the CB of Ag_2O are good reductants that could efficiently reduce the O_2 adsorbed onto the composite catalyst surface into various reactive speices, subsequently leading to the formation of ·OH and oxidation of MO into CO_2, H_2O, etc. Therefore, the enhanced photocatalytic activity is achieved.

4. CONCLUSIONS

In summary, mpg-C_3N_4/Ag_2O nanocomposites have been successfully and directly prepared by a facile, effective, and reproducible method. Under visible light irradiation, the MO photodegradation by the mpg-C_3N_4/Ag_2O nanocomposite was greater than that for mpg-C_3N_4 or Ag_2O alone. More importantly, mpg-C_3N_4/Ag_2O photocatalyst could be reused without loss of photocatalytic activity even after five successive cycles. Therefore, the mpg-C_3N_4/Ag_2O nanocomposite is a promising photocatalytic material for environmental applications as well as water splitting.

Acknowledgment: Financial support from Project supported by the National Natural Science Foundation of China (51572115) and Project supported by the Graduate Science Research Innovation Program Foundation of the Jiangsu Higher Education Institution of China (KYLX15_1040) are gratefully acknowledged.

References and Notes

1. S. Dong, J. Feng, M. Fan, Y. Pi, L. Hu, X. Han, M. Liu, J. Sun, and J. Sun, *RSC Adv.* 5, 14610 (**2015**).
2. Y. Hang, H. B. Yin, Y. Q. Ji, Y. Liu, Z. P. Lu, A. L. Wang, L. Q. Shen, and H. X. Yin, *J. Nanosci. Nanotechnol.* 17, 5539 (**2017**).
3. Y. Hang, H. B. Yin, A. L. Wang, L. Q. Shen, Y. H. Feng, and R. J. Liu, *Water Air Soil Pollut.* 225, 2095 (**2014**).
4. Y. Si, J. C. Huo, H. B. Yin, and A. L. Wang, *J. Nanosci. Nanotechnol.* 18, 3484 (**2018**).
5. D. Fukushi, A. Sato, K. Yoshiola, and M. Kitano, *Bull. Chem. Soc. Jpn.* 90, 885 (**2017**).
6. P. V. Kamat, *J. Phys. Chem. C* 116, 11849 (**2012**).
7. J. X. Low, B. Cheng, and J. G. Yu, *Appl. Surf. Sci.* 392, 658 (**2017**).
8. C. Liu, H. B. Yin, L. P. Shi, A. L. Wang, Y. H. Feng, L. Q. Shen, Z. A. Wu, G. Wu, and T. Jiang, *J. Nanosci. Nanotechnol.* 14, 7072 (**2014**).
9. S. J. A. Moniz, S. A. Shevlin, D. J. Martin, Z. X. Guo, and J. Tang, *Energy Environ. Sci.* 8, 731 (**2015**).
10. K. Maeda and K. Domen, *Bull. Chem. Soc. Jpn.* 89, 627 (**2016**).
11. D. Walsh, N. M. Sanchez-Ballester, V. P. Ting, K. Ariga, and M. T. Weller, *Catal. Sci. Technol.* 6, 3718 (**2016**).
12. M. Pelaez, N. T. Nolan, S. C. Pillai, M. K. Seery, P. Falaras, A. G. Kontos, P. S. M. Dunlop, J. W. J. Hamilton, J. A. Byrne, K. O'Shea, M. H. Entezari, and D. D. Dionysiou, *Appl. Catal. B* 125, 331 (**2012**).
13. R. Fagan, D. E. McCormack, D. D. Dionysiou, and S. C. Pillai, *Mater. Sci. Semicond. Process* 42, 2 (**2016**).
14. X. C. Wang, K. Maeda, A. Thomas1, K. Takanabe, G. Xin, J. M. Carlsson, K. Domen, and M. Antonietti, *Nat. Mater.* 8, 76 (**2009**).
15. Q. Xiang and J. Yu, *J. Phys. Chem. Lett.* 4, 753 (**2013**).
16. J. Liu, Y. Liu, N. Liu, Y. Han, X. Zhang, H. Huang, Y. Lifshitz, S. T. Lee, J. Zhong, and Z. Kang, *Science* 347, 970 (**2015**).
17. S. M. Lyth, Y. Nabae, S. Moriya, S. Kuroki, M. Kakimoto, J. Ozaki, and S. Miyata, *J. Phys. Chem. C* 113, 20148 (**2009**).
18. Z. Zhao, Y. Sun, and F. Dong, *Nanoscale* 7, 15 (**2015**).
19. N. Ding, L. S. Zhang, M. Hashimoto, K. Iwasaki, N. Chikamori, K. Nakata, Y. Z. Xu, J. J. Shi, H. J. Wu, Y. H. Luo, D. M. Li, A. Fujishima, and Q. B. Meng, *J. Colloid Int. Sci.* 512, 474 (**2018**).
20. X. C. Wang, S. Blechert, and M. Antonietti, *ACS Catal.* 2, 1596 (**2012**).
21. X. Jin, V. V. Balasubramanian, S. T. Selvan, D. P. Sawant, M. A. Chari, G. Q. Lu, and A. Vinu, *Angew. Chem. Int. Ed.* 48, 7884 (**2009**).
22. E. Z. Lee, Y. S. Jun, W. H. Hong, A. Thomas, and M. M. Jin, *Angew. Chem. Int. Ed.* 49, 9706 (**2010**).
23. J. Liang, Y. Zheng, J. Chen, J. Liu, D. H. Jurcakova, M. Jaroniec, and S. Z. Qiao, *Angew. Chem.* 51, 3892 (**2012**).
24. Y. J. Cui, J. S. Zhang, G. G. Zhang, J. H. Huang, P. Liu, M. Antonietti, and X. C. Wang, *J. Mater. Chem.* 21, 13032 (**2011**).
25. X. Wang, S. Li, H. Yu, J. Yu, and S. Liu, *Chem. Eur. J.* 17, 7777 (**2011**).
26. D. Sarkar, C. K. Ghosh, S. Mukherjee, and K. K. Chattopadhyay, *ACS Appl. Mater. Interfaces* 5, 331 (**2013**).

27. M. Wu, J. M. Yan, M. Zhao, and Q. Jiang, *ChemPlusChem.* 77, 931 (**2012**).
28. L. Zhu, B. Wei, L. L. Xu, Z. Lu, H. L. Zhang, H. J. Gao, and X. Che, *CrystEngComm.* 14, 5705 (**2012**).
29. C. L. Yu, G. Li, S. Kumar, K. Yang, and R. C. Jin, *Adv. Mater.* 26, 892 (**2014**).
30. S. K. Le, T. S. Jiang, Q. Zhao, X. F. Liu, Y. Y. Li, B. W. Fang, and M. Gong, *Rsc. Adv.* 6, 38811 (**2016**).
31. A. Thomas, A. Fischer, F. Goettmann, M. Antonietti, J. O. Müller, R. Schlögl, and J. M. Carlsson, *J. Mater. Chem.* 18, 4893 (**2008**).
32. M. J. Bojdys, J. O. Müller, M. Antonietti, and A. Thomas, *Chem. Eur. J.* 14, 8177 (**2008**).
33. S. C. Yan, Z. S. Li, and Z. G. Zou, *Langmuir* 25, 10397 (**2009**).
34. S. Kumar, T. Surendar, A. Baruah, and V. Shanker, *J. Mater. Chem. A* 1, 5333 (**2013**).
35. V. N. Khabashesku, J. L. Zimmerman, and J. L. Margrave, *Chem. Mater.* 12, 3264 (**2000**).
36. X. Li, J. Zhang, L. Shen, Y. Ma, W. Lei, Q. Cui, and G. Zou, *Appl. Phys. A* 94, 387 (**2009**).
37. Y. Zhao, Z. Liu, W. Chu, L. Song, Z. Zhang, D. Yu, Y. Tian, S. Xie, and L. Sun, *Adv. Mater.* 20, 1777 (**2008**).
38. M. Xu, L. Han, and S. J. Dong, *ACS Appl. Mater. Interfaces* 5, 12533 (**2013**).
39. S. K. Le, T. S. Jiang, Y. W. Li, Q. Zhao, Y. Y. Li, W. B. Fang, and M. Gong, *Appl. Catal. B* 200, 601 (**2017**).
40. W. Zhou, H. Liu, J. Wang, D. Liu, G. Du, and J. Cui, *Appl. Mater. Interfaces* 2, 2385 (**2010**).
41. Y. F. Zhang, X. J. Bo, A. Nsabimana, C. Luhana, G. Wang, H. Wang, M. Li, and L. P. Guo, *Biosens. Bioelectron.* 53, 250 (**2014**).
42. Q. Zhao, Y. L. Shen, Q. Wang, J. Tian, X. P. Zhou, and T. S. Jiang, *Chem. Eng. J.* 230, 124 (**2013**).
43. G. Liao, S. Chen, X. Quan, H. Yu, and H. Zhao, *J. Mater. Chem.* 22, 2721 (**2012**).
44. C. S. Pan and Y. F. Zhu, *Environ. Sci. Technol.* 44, 5570 (**2010**).

Received: 14 December 2017. Accepted: 28 January 2018.